

Predictive Control of Actively Articulated Mobile Robots Crossing Irregular Terrains

Gustavo Freitas* Fernando Lizarralde* Liu Hsu*

* Dept. of Electrical Eng., COPPE/Federal University of Rio de Janeiro, Brazil (e-mail: gfreitas, fernando, liu@coep.ufrj.br).

Abstract: This paper concerns the reconfiguration control of actively articulated mobile robots navigating through irregular terrains. Active mechanisms are able to accommodate for different operation conditions. The capability to influence mobility depends on the mechanism kinematic structure and the actuators velocity limitations. The robot mobility is evaluated considering ground clearance, orientation and stability. Control strategies are proposed considering the actuators bandwidth to compensate abrupt variations of the navigation trajectory and the driven terrain. The proposed solution consists on anticipating the command action by employing a predictive functional control method to adjust the robot for critical conditions faced during operation. Numerical simulations using field data, recorded while navigating on a natural terrain, are performed to verify the proposed strategies controlling a robot with two actuated DoF.

Keywords: Mobile Robots; Field Robotics; Motion Control Systems; Predictive Control; Multiple-Criterion Optimization.

1. INTRODUCTION

Actively Articulated Mobile Robots (AAMRs) provide superior mobility and performance while navigating through irregular and rough terrains when compared to fixed-design ones. Actuators connected to the mechanism are able to adjust the vehicle's configuration, changing its center of mass (CM_R) position according to the operation conditions. By that, it is possible to adjust the robot ground clearance, orientation, and stability in order to decrease the risk of tip over.

Distinct examples of such robots illustrated in Fig. 1 are the Autonomous Prime Mover (APM) [Singh et al., 2009] and the Environmental Hybrid Robot (EHR) [Freitas et al., 2010].



Fig. 1. Examples of Actively Articulated Mobile Robots.

Even though these robots are designed to drive at low speeds, their actuators have velocity limitations that may prevent them from rapidly adapting to sharp terrain changes, therefore potentially limiting their effectiveness in improving the vehicle mobility. The EHR joint leg, for example, takes approximately 13s to travel its full course. A high acceleration caused, e.g., by one wheel falling in a depression on the ground may tip over the vehicle, unless the event can be predicted and the articulations

actuated before it happens. More generally, all robots with articulated elements have to deal with actuator bandwidth in compensating for terrain irregularities.

Different to the common approach of decreasing the robot speed and reduce dynamic effects, we propose a new strategy for reconfiguration of AAMRs, dealing directly with the system actuation constraints by employing a Model Predictive Control (MPC).

The research focuses on the robot reconfiguration control, computed based on a given navigation trajectory. For simplicity, the localization and navigation problems are not directly considered in this paper.

In this work we apply the MPC strategy to reconfigure an AAMR with two actuated DoF through a Predictive Functional Control (PFC). The strategy feasibility is illustrated via numerical simulations using navigation and terrain models obtained from field experiments, demonstrating the control effectiveness in reducing the robot maximum inclinations and the risk of tipping over.

2. ACTIVELY ARTICULATED MOBILE ROBOT

The configuration of a generic rigid body frame E^j is defined with respect to (wrt) a reference coordinate system E^i by the pose $\mathbf{x}_j^i = (p_j^i, R_j^i)$, where $p_j^i \in \mathbb{R}^3$ is the position and $R_j^i \in SO(3)$ is the rotation matrix. The orientation can be parameterized by roll, pitch and yaw angles $\varphi = [\phi_j, \theta_j, \psi_j]^T$.

The system composed by an AAMR moving on a terrain is represented by three coordinate frames: the robot E^R , the terrain E^θ and an inertial reference E^I . The pose \mathbf{x}_R^I defines the robot configuration wrt the inertial frame, which can be calculated combining \mathbf{x}_θ^I and \mathbf{x}_R^θ :

$$p_R^I = p_\theta^I + R_\theta^I p_R^\theta, \quad R_R^I = R_\theta^I R_R^\theta \quad (1)$$

We assume that the planar navigation trajectory, given by position $[p_{\vartheta x}^I(t), p_{\vartheta y}^I(t)]^T$ and topographic (wrt the local terrain) yaw angle $\psi_{\vartheta}(t)$, is known *a priori* $\forall t$.

The local terrain can be simplified by a single plane defined according to the contact points $p_{ci}, i = 1, \dots, m$ with the robot wheels. Since the terrain variations affect the robot vertical displacement and orientation, it is possible to parametrize the covered profile using the height $h_{\vartheta} = p_{\vartheta z}^I$, and angles $\phi_{\vartheta}, \theta_{\vartheta}$, such that $\vartheta : [h_{\vartheta}, \phi_{\vartheta}, \theta_{\vartheta}]^T$. The driven terrain $\vartheta(l)$ is parameterized wrt the vehicle traveled distance $l(t) = \int_0^t \|\dot{p}_{\vartheta}^I(t)\| dt$.

The considered articulated mechanism is capable of adjusting the CM_R position in the lateral plane of the robot. For that, the robot counts with two 1-DoF actuated legs installed in the body. The robot is represented by a rectangular prism with width L and prismatic joint legs with length d_i . The robot frame E^R coincides with CM_R , as presented in Fig. 2.

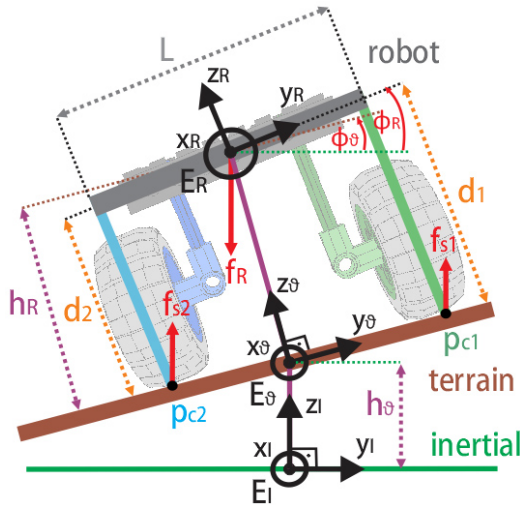


Fig. 2. Model of an actively articulated mobile robot.

The wheel-terrain contact points p_{ci}^R are considered to be located at the legs terminations in terms of the active joints $d = [d_1, d_2]^T$:

$$p_{c1}^R = \begin{bmatrix} 0 \\ \frac{L}{2} \\ -d_1 \end{bmatrix}, \quad p_{c2}^R = \begin{bmatrix} 0 \\ -\frac{L}{2} \\ -d_2 \end{bmatrix} \quad (2)$$

The terrain plane is given by the unit normal vector n_{ϑ}^R and any contact point p_{ci}^R , such as:

$$(n_{\vartheta}^R)^T p_{ci}^R - h_R = 0 \quad (3)$$

where $h_R \in \mathbb{R}$ is the distance between terrain and E^R .

Considering the robot with $m = 2$ contact points, the terrain normal vector n_{ϑ}^R is given by:

$$n_{\vartheta}^R = \begin{bmatrix} 0 \\ -\sin(\delta) \\ -\cos(\delta) \end{bmatrix}, \quad \delta = \arctan\left(\frac{\Delta_d}{L}\right) \quad (4)$$

and $\Delta_d = d_2 - d_1$.

The pose \mathbf{x}_{ϑ}^R corresponds to position

$$p_{\vartheta}^R = h_R n_{\vartheta}^R \quad (5)$$

and orientation $R_{\vartheta}^R = R_x(-\delta) \in SO(3)$.

By deriving and combining poses \mathbf{x}_{ϑ}^I and \mathbf{x}_{ϑ}^R , it is possible to calculate the robot linear v_R^I and angular ω_R^I velocities wrt the inertial frame E^I . The angular velocity can be obtained deriving roll, pitch and yaw angles such that $\omega = J_R \dot{\vartheta}$, where $J_R \in \mathbb{R}^{3 \times 3}$ is the representation jacobian [Goldstein, 1980].

The resulting forces and torques acting on CM_R are estimated using Newton-Euler equations [Murray et al., 1993], such as:

$$\begin{bmatrix} f_r^I \\ \tau_r^I \end{bmatrix} = \begin{bmatrix} M I & 0 \\ 0 & R_R^I \mathcal{I} R_R^I \end{bmatrix} \begin{bmatrix} \dot{v}_R^I \\ \dot{\omega}_R^I \end{bmatrix} + \begin{bmatrix} \omega_k^i \times M v_R^I \\ \omega_k^i \times R_R^I \mathcal{I} R_R^I \omega_R^I \end{bmatrix} \quad (6)$$

where M is the mass, $\mathcal{I} \in \mathbb{R}^{3 \times 3}$ is the robot inertia moment, and identity $I \in \mathbb{R}^{3 \times 3}$. The dynamic is obtained in terms of the navigation trajectory and driven terrain.

3. MOBILITY ANALYSIS

The capability to move throughout the environment determines the system mobility, which can be evaluated considering the robot ground clearance, orientation and stability.

It is important to keep a reference distance from the ground, specially when moving on irregular terrains, in order to avoid collisions with obstacles.

One requirement while transporting people and cargo is to keep the robot body parallel to horizontal. The robot configuration presented in Fig. 3(b) distributes the supporting forces uniformly among the legs, improving wheel traction efficiency. The system is stable, however it is easier to tip over the robot around p_{c2} than p_{c1} .

The most stable configuration is achieved when the robot is inclined in the opposite direction of the terrain, as presented in Fig. 3(c). In this configuration, tip over risk is the same around p_{c1} and p_{c2} . Still, the supporting forces distribution is non uniform, decreasing traction efficiency.

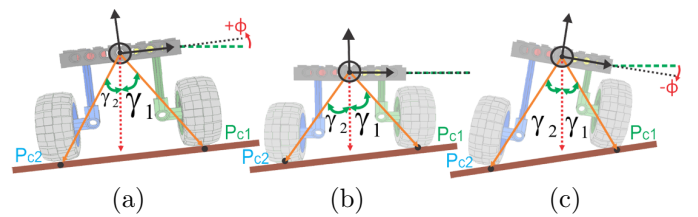


Fig. 3. Orientation and tip over angles for different robot configurations: (a) $\phi_R > 0$ and $\gamma_1 \gg \gamma_2$, (b) $\phi_R = 0$ and $\gamma_1 > \gamma_2$, (c) $\phi_R < 0$ and $\gamma_1 = \gamma_2$.

3.1 Ground Clearance

The minimum distance from the robot frame E^R to the plane representing the terrain corresponds to the vehicle ground clearance h_R , defined by the active joints d :

$$h_R = \frac{L}{2} \frac{\sigma_d}{\sqrt{\Delta_d^2 + L^2}} = f_h(d) \quad (7)$$

with $\sigma_d = d_1 + d_2$.

3.2 Orientation

The robot orientation can be expressed by the rotation matrix R_R^I , or parameterized through roll, pitch and yaw angles $\varphi_R = [\phi_R, \theta_R, \psi_R]^T$.

The orientation R_R^I is composed by two rotations: first R_{ϑ}^I from terrain wrt inercial given by φ_{ϑ} , and second R_R^{ϑ} from the robot wrt the terrain defined by δ (4) according to the active joints d :

$$R_R^I = R_z(\psi_{\vartheta})R_y(\theta_{\vartheta})R_x(\phi_{\vartheta}) R_x(\delta) = f_o(d, \varphi_{\vartheta}) \quad (8)$$

3.3 Stability via Force-Angle Measures

The stability metric proposed in [Papadopoulos and Rey, 1996] takes into account the angles γ_i necessary to rotate the robot until tip over, illustrated in Fig. 3. The angles depend on the system of forces f_i^* acting on CM_R , wrt the tip over axes a_{ti} , given by:

$$f_i^* = (I - a_{ti}a_{ti}^T) f_r^R + \frac{\check{p}_{ci}^R \times n_i}{\|p_{ci}^R\|}, \quad n_i = (a_{ti}a_{ti}^T) \eta_r^R \quad (9)$$

where the tip over axes $a_{t1} = \{x^R\}$ and $a_{t2} = \{-x^R\}$, $\check{p} = \frac{p}{\|p\|}$ is the normalized vector, and f_r, η_r correspond to the resulting forces and torques (6).

Considering the articulated robot with $m = 2$, the tip over angles between f_i^* and p_{ci} are calculated using the geometric relationship:

$$\gamma_i = \sigma_i \cos^{-1} (\check{f}_i^* \cdot \check{p}_{ci}), \quad i = 1, 2 \quad (10)$$

with

$$\sigma_i = \begin{cases} +1, & (\check{f}_i^* \times \check{p}_{ci})^T a_{ti} > 0 \\ -1, & (\check{f}_i^* \times \check{p}_{ci})^T a_{ti} \leq 0 \end{cases}$$

According to the criterion, the stability is estimated by the minimum tip over angle:

$$\beta = \min(\gamma_i), \quad i = 1, \dots, m \quad (11)$$

The system is unstable when $\beta \leq 0$. The most stable configuration is the one where all γ_i have the same value. Thus, considering a robot with even number m of wheels, it is convenient to represent the system stability by the difference $\Delta\gamma$ between opposite tip over angles, such as:

$$\Delta\gamma = \gamma_i - \gamma_{i+m/2} = f_e(d, \varphi_{\vartheta}, f_r, \eta_r) \quad (12)$$

where $\Delta\gamma \in \mathbb{R}^{m/2}$.

4. TERRAIN MODELING

Irregular and rough terrains are, in general, complex nonlinear surfaces not easily modeled [Sreenivasan and Wilcox, 1994]. One solution is to represent the covered terrain as a mesh [Burgard and Hebert, 2008]. This is a compact representation, specially when applying mesh simplification algorithms to reduce the terrain model to a small number of vertices.

The robot mobility metrics presented take into account the contact points with the wheels, and the rest of the terrain profile is disregarded. Thus, it is possible to represent the terrain as a patch of planes defined by the contact points,

corresponding to the minimum resolution employed by the mesh representation.

Most of the work done on mobility prediction assumes knowledge about the positions of the contact points. These positions can be estimated based on the vehicle's geometry and the navigation trajectory. Despite the associated uncertainties, the terrain profile detection is feasible using some adequate sensor suite.

Given the robot traveled distance l , it is possible to compute a plane $\vartheta(l)$ in terms of $p_{ci}^I(l)$, representing the terrain local characteristics. The local plane is defined wrt E^I by the unit normal vector n_{ϑ}^I and any contact point p_{ci}^I , such as:

$$(n_{\vartheta}^I)^T p_{ci}^I - d_{\vartheta} = 0 \quad (13)$$

where $d_{\vartheta} \in \mathbb{R}$ is the distance between E^{ϑ} and E^I .

The terrain frame E^{ϑ} is given by the projection of E^R onto plane ϑ , defined by the position p_{ϑ}^I such that:

$$p_{\vartheta}^I = p_R^I - h_R (n_{\vartheta}^R)^I \quad (14)$$

where the robot position p_R^I is obtained from the contact points p_c^I and active joints length d .

The terrain height h_{ϑ} is calculated with:

$$h_{\vartheta} = [0, 0, 1] p_{\vartheta}^I \quad (15)$$

and the orientation is given by the angles ϕ_{ϑ} and θ_{ϑ} , obtained from the normal vector n_{ϑ}^I :

$$\phi_{\vartheta} = \arctan \left(\frac{-n_{\vartheta}^I y}{n_{\vartheta}^I z} \right), \quad \theta_{\vartheta} = \arctan \left(\frac{n_{\vartheta}^I x}{\sqrt{(n_{\vartheta}^I y)^2 + (n_{\vartheta}^I z)^2}} \right) \quad (16)$$

Now considering that the vehicle is traveling along a given path through the terrain, it is possible to parameterize the covered planes wrt the vehicle traveled distance l as:

$$\vartheta(l) : [h_{\vartheta}, \phi_{\vartheta}, \theta_{\vartheta}]^T = f_{\vartheta}(l) \quad (17)$$

4.1 Field Experiment

This section describes the terrain field experiments accomplished with one agricultural platform (Fig. 4) from the Autonomous Prime Movers (APM) family, designed at the Robotics Institute - Carnegie Mellon University as part of the CASC project [Singh et al., 2009].

The base vehicle is the APM "Laurel", employing a high-accuracy Applanix POS 220 LV INS/GPS with 6 DoF localization system and a Sick LMS 291 laser scanner installed in a push-broom configuration ($\theta_L = 20^\circ$) to measure the terrain profile at approximately 4m ahead of the robot.

Here we consider a field experiment accomplished with Laurel at Soergel orchard (PA-EUA) on 24/08/2011. During the test, the APM collected data from the embedded sensors while crossing an irregular terrain partially covered by grass. The obtained model is presented in Fig. 5, highlighting the contact points and also the sequence of planes representing the driven terrain. More details about laser data registration is presented in [Freitas et al., 2012].

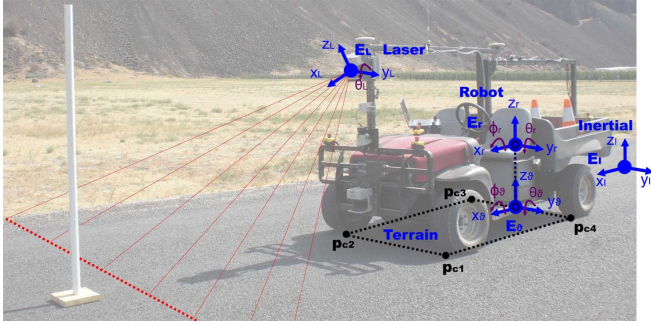


Fig. 4. Autonomous Prime Mover Laurel employing a localization system and a laser scanner for terrain modeling. The image illustrates the coordinate frames from laser E^L , robot E^R , terrain E^T e inertial reference E^I .

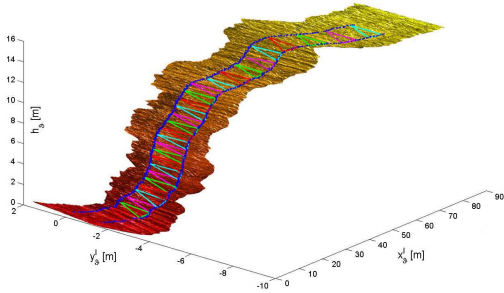


Fig. 5. Natural terrain model given by a sequence of planes $\vartheta(l)$ based on the contact points $p_{ci}^T(l)$ with the robot wheels moving at Soergel orchard.

Figure 6 illustrates the terrain parametrization $\vartheta(l)$ computed with experimental data obtained by Laurel during the operation at Soergel orchard.

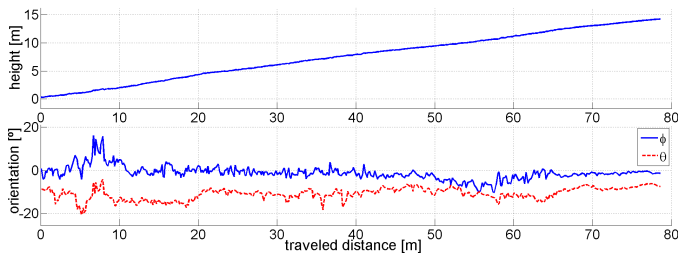


Fig. 6. Terrain parametrization $\vartheta(l) = [h_\vartheta, \phi_\vartheta, \theta_\vartheta]^T$ obtained during field operation.

5. RECONFIGURATION BASED ON PREDICTIVE FUNCTIONAL CONTROL

The Predictive Functional Control (PFC) was proposed in [Richalet, 1993b] to deal with fast processes, including trajectory tracking of 2 DoF turret [Richalet, 1993a] and 4 DoF parallel manipulator [Vivas and Poignet, 2005]. Another application is the steering control of an agricultural tractor in presence of sliding, reducing overshoots at beginning of curves induced by actuation delays and vehicle large inertia [Lenain et al., 2005].

Similar to the MPC approach, the PFC can be divided into three stages [Camacho and Bordons, 2004]: first it predicts the process outputs at future instants based on the given model; second it optimizes a cost function to

obtain the control sequence; then the first term of the control sequence is applied to command the joints.

The PFC main characteristic is to evaluate costs considering the predicted errors only regarding specific points of the future horizon; these coincident points are chosen here according to the harsh mobility conditions faced during operation.

The system is represented by a discrete state-space model. Considering the AAMR with d active joints and the kinematic control action defined as $u = \dot{d}$, the resulting model is given by:

$$d(k+1) = d(k) + \Delta t u(k) \quad (18)$$

$$y(k) = f(d(k), \varphi_\vartheta(k), f_r(k), \eta_r(k)) \quad (19)$$

where $d \in \mathbb{R}^{n_a}$ is the state, $\Delta t \in \mathbb{R}$ is a temporal increment, $u \in \mathbb{R}^{n_a}$ is the command action sent to the actuators, and $y \in \mathbb{R}^{n_a}$ is the measured system output, corresponding to the mobility metrics - ground clearance, orientation, stability - to be controlled.

In general, predictive strategies anticipate the control command such that the system predicted output tracks a reference trajectory r defined for a future time horizon t_h . PFC places the desired closed-loop dynamic into the reference trajectory, equivalent to a first order lag filter approach. The closed-loop set points are defined by w :

$$w(k+i) = r(k+i) - \alpha^i(r(k) - \hat{y}(k)), \quad 0 \leq i \leq t_h \quad (20)$$

where $0 < \alpha < 1$ sets the system closed-loop pole; given the sample period T and the system closed-loop time constant τ , we have $\alpha = e^{-\frac{T}{\tau}}$.

The coincident points are defined as $w(k+n_i)$, where $n_i \in N_i$ and $N_i = \{n_1, n_2, \dots, n_h\}$. The number of points n_h is limited by the sampling time: a small n_h may not represent the system dynamic behavior; on the other hand, a large n_h requires more processing power to optimize the cost function.

For articulated mobile robots navigating through irregular and rough terrains, the coincident points can be selected considering peaks in the reference trajectory. The choice uses Δw , such that:

$$N_i = \{n_i \in [0, t_h] \mid \Delta w(k+n_i) \Delta w(k+n_i-1) \leq 0\} \quad (21)$$

The control law is computed using a deadbeat strategy to enforce equality of the system output prediction \hat{y} and the reference trajectory w at the coincident points:

$$\hat{y}(k+n_i) = w(k+n_i), \quad n_i = n_1, n_2, \dots, n_h \quad (22)$$

The control performance is evaluated through a cost J defined as the quadratic sum of the errors between the predicted system output \hat{y} and the reference trajectory w , wrt the coincident points, by the objective function:

$$J = \sum_{n_i=n_1}^{n_h} (\hat{y}(k+n_i) - w(k+n_i))^2 + \lambda (u(k))^2 \quad (23)$$

and the term multiplied by λ associates costs to the control action, working as a smoothing control term in the objective function.

Considering the first order system (18-19), it is possible to compute the control signal by the weighting factors μ , defined wrt each contact point, such that:

$$u(k+n_i) = \mu(n_i), \quad n_i = 0, n_1, n_2, \dots, n_h \quad (24)$$

It is important to notice that the command signal stays constant between the coincident points, such that $u \in \mathbb{R}^{n_a \times n_h}$.

Applying the control signal (24), the system predicted output \hat{y} is calculated wrt the coincident points $N_i = \{n_1, n_2, \dots, n_h\}$:

$$\begin{aligned} \hat{d}(k+n_{i+1}) &= d(k+n_{i-1}) + \Delta t(n_{i+1} - n_i)u(k+n_i) \\ \hat{y}(k+n_i) &= f(\hat{d}(k+n_i), \varphi_{\vartheta}(k+n_i), f_r(k+n_i), \eta_r(k+n_i)) \end{aligned}$$

The future control sequence is obtained by an optimizer that, given the system constraints, returns optimal weighting factors to minimize cost J .

The applied command signal corresponds to the first term of the control sequence $u(k) = \mu(0)$, while the rest of the sequence is used as an initial guess to optimize cost J during the next algorithm iteration.

The PFC tuning parameters are the desired closed-loop time constant defined by α , the prediction time horizon t_h , and the choice of coincident points N_i . The PFC implementation is summarized by algorithm (1).

Algorithm 1 PFC Algorithm

```

1: initialize parameters:  $t_h, \alpha, u(0) = 0$ 
2: for  $k = 0 \rightarrow t$  do
3:   for  $i = 0 \rightarrow t_h$  do
4:     calculate  $\hat{d}(k+i)$  with  $u(k+i-1)$ 
5:     calculate  $\hat{y}(k+i)$  with  $\hat{d}(k+i)$ 
6:     calculate  $w(k+i)$  with  $\hat{y}(k+i)$  using (20)
7:     obtain the coincident points with  $w(k+i)$  using (21)
8:   end for
9:   procedure optimizeCostJ( $\mu(k)$ )
10:    adjust  $\mu(k+1)$  to minimize  $J$ , given the constraint  $|\dot{d}|_{\max}$ 
11:   end procedure
12:   define the actuator command  $u(k)$  as  $\mu(0)$ 
13: end for

```

The AAMR with 2 actuated DoF presented in Fig. 2 is capable of controlling two mobility criteria. One degree of articulation is constrained to maintain the reference distance between robot and terrain; otherwise, the achieved configurations may be inconsistent. The other articulation can be applied to adjust orientation or stability.

5.1 Ground Clearance and Orientation Control

The system model (19) considers the output:

$$y = \begin{bmatrix} h_R \\ \phi_R \end{bmatrix} = f(d, \varphi_{\vartheta})$$

The control objective is to keep the reference ground clearance h_R^* and track the orientation desired closed-loop dynamic w_{ϕ} (20) defined with $\phi_R^* = 0$ as reference r . The objective function is given by:

$$J = \sum_{n_i=n_1}^{n_h} \left[(\hat{h}_R(k+n_i) - h_R^*)^2 + (\hat{\phi}_R(k+n_i) - w_{\phi}(k+n_i))^2 \right] \quad (25)$$

5.2 Ground Clearance and Stability Control

The system model (19) considers the output:

$$y = \begin{bmatrix} h_R \\ \Delta\gamma \end{bmatrix} = f(d, \varphi_{\vartheta}, f_r, \eta_r)$$

The control objective is to keep the reference ground clearance h_R^* and track the stability desired closed-loop dynamic $w_{\Delta\gamma}$ (20) defined with $\Delta^*\gamma = 0$ as reference r . The objective function is given by:

$$J = \sum_{n_i=n_1}^{n_h} \left[(\hat{h}_R(k+n_i) - h_R^*)^2 + \left(\frac{\hat{\Delta}\gamma(k+n_i) - w_{\Delta\gamma}(k+n_i)}{\beta(k+n_i)} \right)^2 \right] \quad (26)$$

The division by term β increases the cost associated to configurations with small tip over angles. Rollover happens when $\beta = 0$, resulting in infinite cost.

6. SIMULATION RESULTS

To assess the feasibility of the proposed reconfiguration control strategies, simulations with the AAMR are accomplished. Experimental data collected by the APM during the field operation previously described is employed to model the driven terrain profile presented in Fig. 6 and the planar navigation trajectory illustrated in Fig. 7.

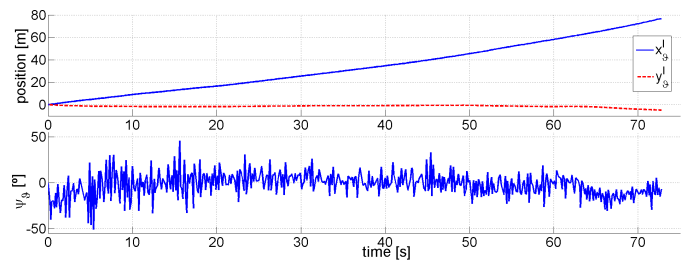


Fig. 7. Planar navigation trajectory defined by position $[p_{\vartheta x}^I(t), p_{\vartheta y}^I(t)]^T$ and orientation $\psi_{\vartheta}(t)$ executed during field operation.

The robot parameters are: length $L = 100\text{cm}$, mass $M = 100\text{kg}$ and inertia moment $\mathcal{I} = \text{diag}([8.42, 0.17, 8.42])\text{kg}\cdot\text{m}^2$. The actuators constraints are given by $\dot{d} \leq 10\text{cm/s}$. The reference height $h_R^* = 60\text{cm}$ defines the robot standard configuration with $d_1 = d_2 = 60\text{cm}$. The presented results correspond to the traveling distance of $l(t) \in [0, 13.4]\text{m}$.

All simulations were accomplished using sampling time of $T = 0.02\text{s}$; the desired closed-loop dynamic w is defined by $\alpha = 0.15$. The prediction horizon is defined considering the actuators bandwidth and reference variations. The applied objective function (23) does not associate costs to the control action, such that $\lambda = 0$. The coincident points are chosen to satisfy inequality (21). The results obtained with the PFC are compared to the high gain proportional control strategy proposed in [Freitas et al., 2010].

Figure 8 illustrates the ground clearance and orientation control applied to the AAMR. The PFC control signal is defined optimizing the cost function J (25), wrt the coincident points marked in the figure by stars.

For the prediction horizon $t_h = 3.0\text{ s}$, the associated costs rise between the instants $t = [4, 7]\text{s}$ due to the terrain abrupt variation overridden at $t = 7\text{s}$. The maximum cost J reaches 165 at $t = 4.5\text{s}$ with the proportional strategy; the value decreases to 90 at $t = 5.7\text{s}$ using the PFC control.

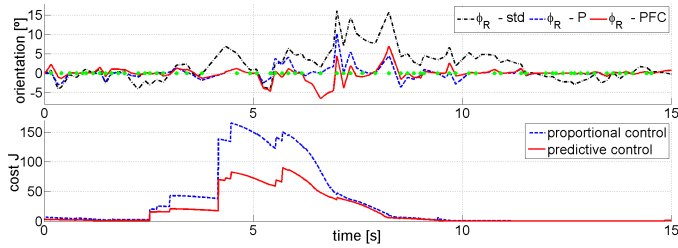


Fig. 8. (upper) Robot orientation ϕ_R achieved in standard configuration (std), or applying the proportional (P) or predictive (PFC) control strategies. (bottom) Associated cost J .

The terrain maximum inclination of $\phi_\theta = 16^\circ$ at $t = 7s$ is attenuated to $\phi_R = 10.1^\circ$ with the proportional control; the predictive strategy reduces the maximum inclination to $\phi_R = 6.9^\circ$ at $t = 8.2s$. Regarding stability, the critical value achieved by the PFC is $\Delta\gamma = 47.8^\circ$ at $t = 9.7s$.

Figure 9 illustrates the ground clearance and stability control applied to the AAMR. The PFC control signal is defined optimizing the cost function J (26), wrt the coincident points marked in the figure by stars.

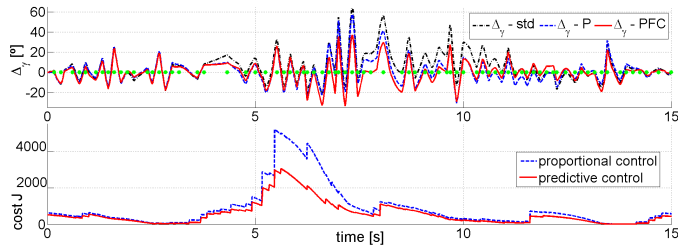


Fig. 9. (upper) Robot stability metric $\Delta\gamma$ achieved in standard configuration (std), or applying the proportional (P) or predictive (PFC) control strategies. (bottom) Associated cost J .

For the prediction horizon $t_h = 2.0$ s, the maximum cost J reaches 5.2×10^3 at $t = 5.5s$ with the proportional strategy; the value decreases to 3.0×10^3 at $t = 5.6s$ using the PFC.

The maximum difference between tip over angles $\Delta\gamma = 63.8^\circ$ ($\beta = 6.1^\circ$) achieved at $t = 7.3s$ by the robot in standard configuration is attenuated to $\Delta\gamma = 57.5^\circ$ ($\beta = 9.5^\circ$) with the proportional control; the predictive strategy reduces the maximum difference to $\Delta\gamma = 36.5^\circ$ ($\beta = 21.5^\circ$) at the same instant. Regarding orientation, the critical value achieved by the PFC is $|\phi_R| = 10.6^\circ$ at $t = 9.4s$.

The results are summarized in Table 1, presenting critical mobility values achieved by the robot in standard configuration, or applying the PFC control strategies. The stability increments are calculated wrt to minimum β reached by the robot in standard configuration.

	std config.	height & orientation	height & stability
$ \Delta_h _{\max}$ [cm]	0.0	0.3	1.6
$ \phi_R _{\max}$ [°]	16.0	6.9	10.6
$ \Delta\gamma _{\max}$ [°]	63.8	47.8	36.5
β_{\min} [°]	6.1	15.5	21.5
Stability Increment		154 %	252 %

Table 1. PFC simulation results.

7. CONCLUSION AND FUTURE WORK

The PFC strategy achieves significant mobility enhancements when controlling the AAMR navigating through a terrain based on actual field data. For the given scenario, the predictive control is capable of reducing the robot maximum inclination from $\phi_R = 16^\circ$ to $\phi_R = 6.9^\circ$; the proportional control only attenuates the value to $\phi_R = 10.1^\circ$, even using high gain and saturating the actuators. From the stability viewpoint, the critical tip over angle of $\beta = 6.1^\circ$ achieved by the robot in standard configuration rises to $\beta = 21.5^\circ$; the proportional control commands the actuators achieving $\beta = 9.5^\circ$: the performance difference between both methods is about 200% wrt the standard configuration.

The results obtained so far are based on simulations; the next step consists on implementing and verifying the predictive control with a real AAMR. The case study considers a 2 actuated DoF mechanism executing a specific trajectory in a given irregular terrain. As future work, the proposed control strategy will be scalable to highly articulated robots, including exploration rovers and explosive ordnance disposal (EOD) robots. Other future line of research consists on dealing with different mobility factors, e.g., wheel traction efficiency.

ACKNOWLEDGEMENTS

This work was partially supported by CNPq, Brazil. The authors wish to thank all members of the Comprehensive Automation for Specialty Crops project, particularly Profs. Marcel Bergerman and Sanjiv Singh.

REFERENCES

- W. Burgard and M. Hebert. World Modeling. *Handbook of Robotics*, pages 853–870, 2008.
- E. F. Camacho and C. Bordons. *Model predictive control*. Springer Verlag, 2004.
- G. Freitas, G. Gleizer, F. Lizarralde, L. Hsu, and N. R. Salvi dos Reis. Kinematic reconfigurability control for an environmental mobile robot operating in the amazon rain forest. In *Journal of Field Robotics*, volume 27, pages 197–216, March - April 2010.
- G. Freitas, B. Hamner, M. Bergerman, and S. Singh. A practical obstacle detection system for autonomous orchard vehicles. In *IEEE/RSJ Int. Conf. on Intelligent Robots and Systems*, Algarve, Portugal, October 2012.
- H. Goldstein. *Classical Mechanics*. Columbia University, 1980.
- R. Lenain, B. Thuilot, C. Cariou, and P. Martinet. Model predictive control for vehicle guidance in presence of sliding: application to farm vehicles path tracking. In *Proc. of IEEE Int. Conf. on Robotics & Automation*, pages 885–890. IEEE, 2005.
- R. M. Murray, Z. Li, and S. S. Sastry. *A Mathematical Introduction to Robotic Manipulation*. CRC, 1993.
- E. G. Papadopoulos and D. A. Rey. A new measure of tipover stability margin for mobile manipulators. In *Proc. of IEEE Int. Conf. on Robotics & Automation*, volume 4, pages 3111–3116, Minneapolis (MN), April 1996.
- J. Richalet. Industrial applications of model based predictive control. *Automatica*, 29(5):1251–1274, 1993a.
- J. Richalet. Pratique de la commande prédictive. *Hermès*, 1993b.
- S. Singh, T. Baugher, M. Bergerman, K. Ellis, B. Grocholsky, B. Hamner, J. Harper, G.A. Hoheisel, L. Hull, and V. Jones. Automation for specialty crops: A comprehensive strategy, current results, and future goals. In *IFAC Int. Workshop on Bio-Robotics, Information Technology, and Intelligent Control for Bioproduction Systems*, Champaign, 2009.
- S. V. Sreenivasan and B. H. Wilcox. Stability and traction control of an actively actuated micro-rover. *Journal of Robotic Systems*, 11(6):487–502, 1994.
- A. Vivas and P. Poignet. Predictive functional control of a parallel robot. *Control Engineering Practice*, 13(7):863–874, 2005.